1991

Hamiltonian Chaos II

Niraj Srivastava
University of Rhode Island

Charles Kaufman
University of Rhode Island, chuck@uri.edu

Gerhard Müller
University of Rhode Island, gmuller@uri.edu

Citation/Publisher Attribution

N. Srivastava, C. Kaufman and G. Müller. *Hamiltonian chaos II*. Computers in Physics **5** (1991), 239-243. Available at: http://dx.doi.org/10.1063/1.4822981

Hamiltonian Chaos II

Niraj Srivastava, Charles Kaufman and Gerhard Müller

Department of Physics, University of Rhode Island, Kingston, RI 02881-0817.

Newton, Lagrange, Hamilton, Poisson. These pioneers who formulated classical mechanics in ever more elegant terms were unaware of the trouble lying ahead. Poincaré was the first to see the abyss, but the warning he expressed received little attention during his lifetime. Two years after his death in 1912, chaos became the new paradigm in Europe ... in everything except mechanics. The formulation of quantum mechanics in the 1920's by Heisenberg, Schrödinger and Dirac further delayed an upheaval in classical mechanics by provoking a revolution in physics. It swept classical dynamics with its potentially interesting but yet little understood peculiarities into limbo for some 50 years. Recently the long-ignored trouble spots of classical mechanics have come back with a vengeance. The profound implications of chaos in nonlinear dynamics are apt to undermine our understanding of quantum mechanics.

Our goal is to illustrate classical and quantum manifestations of Hamiltonian chaos with some simple models of nonlinear dynamics. The emphasis is on the use of modern computational tools both to visualize the connection between theoretical integrability criteria and phenomenological manifestations of chaos and to establish a link as best we can between classical Hamiltonian chaos and quantum nonintegrability effects.

"Where the action is, there is no chaos." This paradoxical statement is true in Hamiltonian dynamics. The integrability of systems with two degrees of freedom depends on the existence of a second integral of the motion $I(q_1, q_2, p_1, p_2)$ in addition to the Hamiltonian $H(q_1, q_2, p_1, p_2)$. There are far-reaching geometric and analytic consequences of the existence of this second integral.[1] The entire four-dimensional $(4d)$ phase space is densely foliated by $2d$ invariant tori, and the Hamiltonian is expressible as a function $H(J_1, J_2)$ of two global action variables J_1, J_2. There exists a canonical transformation under which the canonical equations

$$\dot{q}_i = \frac{\partial H}{\partial p_i}, \qquad \dot{p}_i = -\frac{\partial H}{\partial q_i}, \qquad i = 1, 2 \tag{1}$$

turn into the equations

$$\dot{\phi}_i = \frac{\partial H}{\partial J_i} = \omega_i(J_1, J_2), \qquad \dot{J}_i = -\frac{\partial H}{\partial \phi_i} = 0, \qquad i = 1, 2 \tag{2}$$

for the action-angle coordinates J_i, ϕ_i. The solution of (2) is manifestly straightforward and amounts to a solution of the original dynamical problem. The constraints on the time evolution imposed by the second integral of the motion are thus extremely stringent, leaving literally no room for chaos.

The situation is drastically yet subtly different in nonintegrable systems. Here the foliation of invariant tori is no longer dense anywhere in phase space, and action variables only exist locally for the surviving tori. The Hamiltonian is no longer a smooth function of these local actions, and eqs. (2) are meaningless. The space between intact tori is now filled with chaotic trajectories.

The Poincaré map of phase-space trajectories is a powerful tool for the analysis and visualization of these contrasting situations as they arise in classical Hamiltonian systems. The corresponding quantum system, on the other hand, is most naturally described in terms of its stationary states, the eigenfunctions of its Hamiltonian operator. Therefore, if our ultimate goal is to demonstrate quantum nonintegrability effects that can be identified as direct consequences of classical Hamiltonian chaos, we have to deal with a mismatch in perspective. This mismatch necessitates a refinement of our method of numerical analysis and graphical representation.

There surely exists a bridge between quantum and classical mechanics, but the path over it is shrouded in mist. The challenge is to locate a position on that metaphorical bridge from which both shorelines can be observed with sufficient clarity. Our search for that vantage point has led us to the study of invariants under very general circumstances.[2,3] Invariants play an important role in both classical and quantum mechanics. They can be constructed, as we shall see, for integrable and nonintegrable systems alike. The crucial point is that classical invariants constructed from phase-space trajectories can be directly compared with quantum invariants constructed from wave functions of energy eigenstates, and both types of invariants exhibit nonintegrability effects that are as striking as those we have observed in Poincaré maps.

We first consider a classical system with one degree of freedom, the simple pendulum, specified by the Hamiltonian

$$H(q,p) = \frac{p^2}{2M} + \Gamma(1-\cos q) \tag{3}$$

with $q = \theta$, $p = M\dot{\theta}$, $M = mL^2$, and $\Gamma = mgL$. The time evolution of this system is determined by the canonical equations

$$\dot{q} = p/M, \qquad \dot{p} = -\Gamma \sin q. \tag{4}$$

They are equivalent to the more familiar Lagrange equation for the angular coordinate $\theta(t)$, i.e., $\ddot{\theta} = -(g/L)\sin\theta$. The analytic solution of (4) represents a classic problem in mechanics.[4]

Fig. 1 depicts the familiar phase portrait of the simple pendulum. We have chosen unit such that $M = 1$ and $\Gamma = 1$. Individual curves represent phase-space trajectories at different values of the energy $E = H(q,p)$. The curves represent $1d$ invariant tori in a $2d$ phase space. For $0 < E < 2$, the pendulum undergoes librational motion that is described by the closed curves in the center of the phase portrait. For $E > 2$, the pendulum mass rotates clockwise or anticlockwise around its pivot with nonuniform angular velocity $\dot{\theta}$, and is described by the open curves.

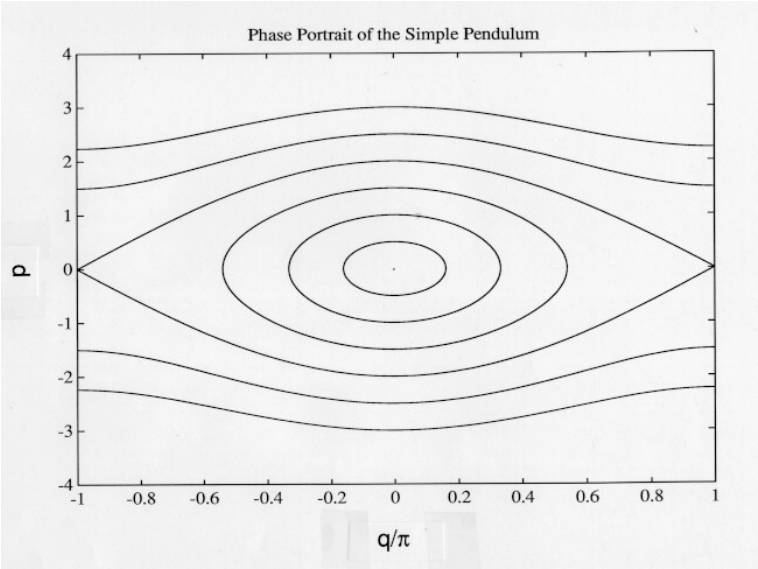

Figure 1: Phase portrait of the simple pendulum. The angular momentum $p = M\dot{\theta}$ is plotted versus the angular coordinate $q = \theta$ for different values of the energy E. We use units such that $M = 1$ and $\Gamma = 1$.

The integrability of Hamiltonian systems with one degree of freedom is always guaranteed. Only one integral of the motion (analytic invariant) is required, and that is provided by the Hamiltonian (energy function) as part of the system specification. No more than one independent analytic invariant can exist, but the choice of the invariant is not unique. The energy function is a special choice that we happen to know analytically.

For the simple pendulum we can construct as many analytic invariants as we wish—they will all be piecewise smooth functions of the energy. Take an arbitrary dynamical variable $A(t)$, such as the kinetic energy $K(t) = \frac{1}{2}M\dot{\theta}^2(t)$, and evaluate the time average over individual (periodic) trajectories:

$$<A> = \frac{1}{\tau(E)}\int_0^{\tau(E)} dt\, A(t) = \overline{I}_A(q_0, p_0) = I_A(E). \tag{5}$$

The integration is over one period $\tau(E)$ of libration or rotation. The result is a piecewise smooth function of E, an analytic invariant that is, as expected, not independent of $H(q, p)$.

A special analytic invariant results from (5) if we choose $A(t) = p(t)\dot{q}(t)$. The time integral (5) then yields the action variable

$$J(E) = \frac{1}{2\pi}\oint p\, dq = \frac{\tau(E)}{2\pi} <p(t)\dot{q}(t)>. \tag{6}$$

The integral $\oint pdq$ corresponds to the area inside the closed curve or between

the open curve and the q-axis in Fig. 1. According to the Liouville theorem,[4] this area is invariant under a canonical transformation, specifically the one to action-angle coordinates (J, ϕ). Eq. (6) then follows directly from the property that the action coordinate is constant on the torus and the angle coordinate goes full circle once around the torus. For open curves the integral $\oint pdq$ contains an undetermined additive constant. We choose the value of that constant such that the action is continuous at the separatrix.

Fig. 2 shows the function $J(E)$ as determined computationally by the above prescription. Remember that $E(J)$ contains important dynamical information: $dE/dJ = \omega(E) = 2\pi/\tau(E)$ is the angular frequency of the periodic trajectory at energy E. The curve $J(E)$ has a weak singularity (infinite slope) at $E = 2$. It implies that $\omega(E) \to 0$ at the separatrix between librational and rotational tori. Also shown in Fig. 2 is the analytic invariant $I_K(E) = <K(t)>$ as constructed computationally from (5). The average kinetic energy I_K is a piecewise smooth function of E and goes to zero at the separatrix. At this energy, the pendulum bob either rests in unstable equilibrium at $\theta = \pi$, or approaches this angle asymptotically for $t \to \tau(E) = \infty$. Note that in this example the ratio $I_K(I)/J(E)$ is inversely proportional to the period $\tau(E)$.

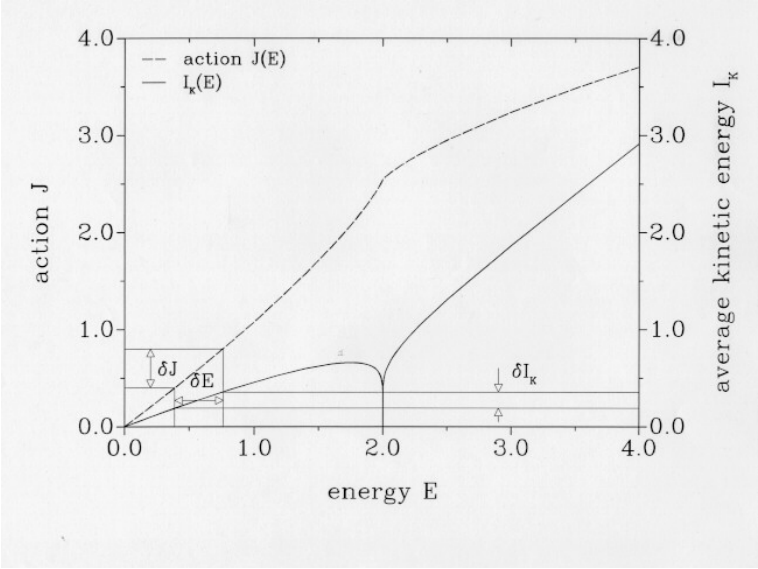

Figure 2: The E-dependence of the analytic invariant $I_K = <K(t)>$ and action variable J for the simple pendulum. The two functions have been computed from (5) and (6), respectively. On the left vertical axis we have specified one interval δJ of an arbitrary linear scale for J. The uniform spacings δJ of this linear scale map onto nonuniform spacings δE on the lower horizontal axis for the variable E and onto nonuniform spacings δI_K on the right vertical axis for the variable I_K.

Any analytic invariant including the energy E can be expressed as a function of the action J. The J-dependence of I_K and E can be visualized by the graphical construction of Fig. 2. We define a linear scale on the J-axis with a length unit δJ. Only one interval δJ is plotted on the left vertical axis. This linear scale is then mapped onto a scale with nonuniform spacing δE along the E-axis and onto another scale with nonuniform spacings δI_K along the I_K-axis. This prescription is carried out for only one unit in Fig. 2. The tick marks of the resulting linear and nonlinear scales have a direct interpretation in the context of semiclassical quantization. The prescription for quantized actions is $J_m = m\hbar + \alpha$, $m = 0, 1, 2, \ldots$, i.e., $\delta J = \hbar$. The constant α is the Maslov index. In general, α has different values on the two sides of a separatrix. Given the correct quantized actions, the tick marks of the resulting nonlinear scales on the other two axes represent the (discrete) spectra of the quantum invariants E and I_K, respectively. These spectra are the eigenvalues of energy and the expectation values (diagonal matrix elements) of the operator K in the energy representation. The study of these quantum invariants will be the focus of a later column.

For classical systems with one degree of freedom, the main results are that:

- Every invariant torus is specified by exactly one analytic invariant. This invariant can be the energy as obtained from (3), the action as obtained from (6), or any time average $<A>$ as obtained from (5).
- The relationship between any two such invariants is expressible in terms of a piecewise smooth function of one variable, such as $J(E)$ and $I_A(E)$.

We now apply the same type of analysis to systems with two degrees of freedom. The extent to which this analysis is possible depends on whether the system is integrable or not. Integrability is no longer satisfied automatically. In part I[1] we discussed a system of two classical spins

$$\vec{S}_i = S(\sin\theta_i \cos\phi_i, \sin\theta_i \sin\phi_i, \cos\theta_i), \qquad i = 1, 2 \tag{7}$$

specified by the energy function

$$H = \sum_{\alpha=\{x,y,z\}} \left[-J_\alpha S_{1\alpha} S_{2\alpha} + \frac{1}{2} A_\alpha ({S_{1\alpha}}^2 + {S_{2\alpha}}^2) \right] \tag{8}$$

and by the equations of motion[3,5] $d\vec{S}_i/dt = -\vec{S}_i \times \partial H/\partial \vec{S}_i$. Each spin represents one degree of freedom expressible, for example, in terms of the pair of canonical coordinates $p_i = S\cos\theta_i$, $q_i = \phi_i$. The integrability condition is nontrivial and depends on the parameters J_α, A_α.[1,5]

For an integrable case of this spin system, there exist exactly two independent analytic invariants. The energy function (8) is one of them. Other analytic invariants can again be constructed numerically via time integrals, but the situation is now considerably more complex than it was for systems with one degree of freedom. Almost all phase-space trajectories are no longer periodic. Instead they wind quasiperiodically around $2d$ invariant tori. Pick any dynamical variable $A(t)$ that is independent of the energy function $H(\vec{S}_1, \vec{S}_2)$ and determine

its time average over the trajectory specified by the initial condition $(\vec{S}_1, \vec{S}_2)$:

$$<A> = \lim_{T\to\infty} \frac{1}{T}\int_0^T dt\, A(t; \vec{S}_1, \vec{S}_2) = \overline{I}_A(\vec{S}_1, \vec{S}_2) = I_A(J_1, J_2). \tag{9}$$

This definition is a generalization of (5), which was applicable for $1d$ tori (periodic trajectories), and yielded a piecewise smooth function of a single variable (E or J). The more general definition (9) applied to an integrable case of our two-spin model yields a piecewise smooth function of two variables, the two action variables that specify individual $2d$ tori. There is no simple generalization of (6) to systems with more than one degree of freedom. We know that global action variables J_1, J_2 do exist and that any invariant $<A>$ is expressible as a piecewise smooth function of them. However, we do not know the values of J_1, J_2 on a given torus.

Consider the two analytic invariants $\tilde{M}_x \equiv \sqrt{<M_x^2>}$ and $\tilde{M}_z \equiv \sqrt{<M_z^2>}$ for our two-spin model as determined from (9), where $M_\mu = (S_1^\mu + S_2^\mu)/2$. The energy function $E = H(\vec{S}_1, \vec{S}_2)$ given by (8) is a third analytic invariant. Since only two invariants can be independent, there must exist an *equation of state*

$$E = E(\tilde{M}_x, \tilde{M}_z) \tag{10}$$

that is represented by a piecewise smooth surface in $(\tilde{M}_x, \tilde{M}_z, E)$-space. Every point on this *invariant-surface* is the image of a point on the action plane (J_1, J_2). This property is illustrated in Figs. 3a and 4a for the integrable case $J_x = 1.2, J_y = 0.8, J_z = 0$, $A_x = A_y = A_z = 0$. The Poincaré map (p_1 versus q_1 for $p_2 = 0, \dot{p}_2 > 0$) is shown in Fig. 3a for several different trajectories at energy $E = 0.2$. The picture illustrates what is known exactly—all tori are intact. Every line depicts a $2d$ torus intersected by the plane $p_2 = 0$. Each torus is represented by a single point in the action plane and a single point on the invariant-surface (10) at $E = 0.2$. In Fig. 4a we show an image of the invariant-surface projected onto the $(E, \tilde{M}_z)$-plane. In the inset to Fig. 4a we also show the section at $E = 0.2$ (indicated by an arrow) of the unprojected surface. All points fall unto a piecewise smooth line as expected. The cusps represent singularities in the (not explicitly known) functional dependence of $\tilde{M}_x, \tilde{M}_z$ on J_1,J_2.

If we could determine, along with the invariants $E, \tilde{M}_x, \tilde{M}_z$, the two action variables J_1,J_2 for each torus, then we could proceed as we did for the simple pendulum. We would define a linear scale in the action plane, in the form of a square grid. This grid, mapped onto the invariant-surface, would become a curvilinear grid of lines of constant action. This procedure is difficult to implement in classical mechanics, but quantum mechanics produces such a topographical map of actions almost for free, as we shall see in part III.

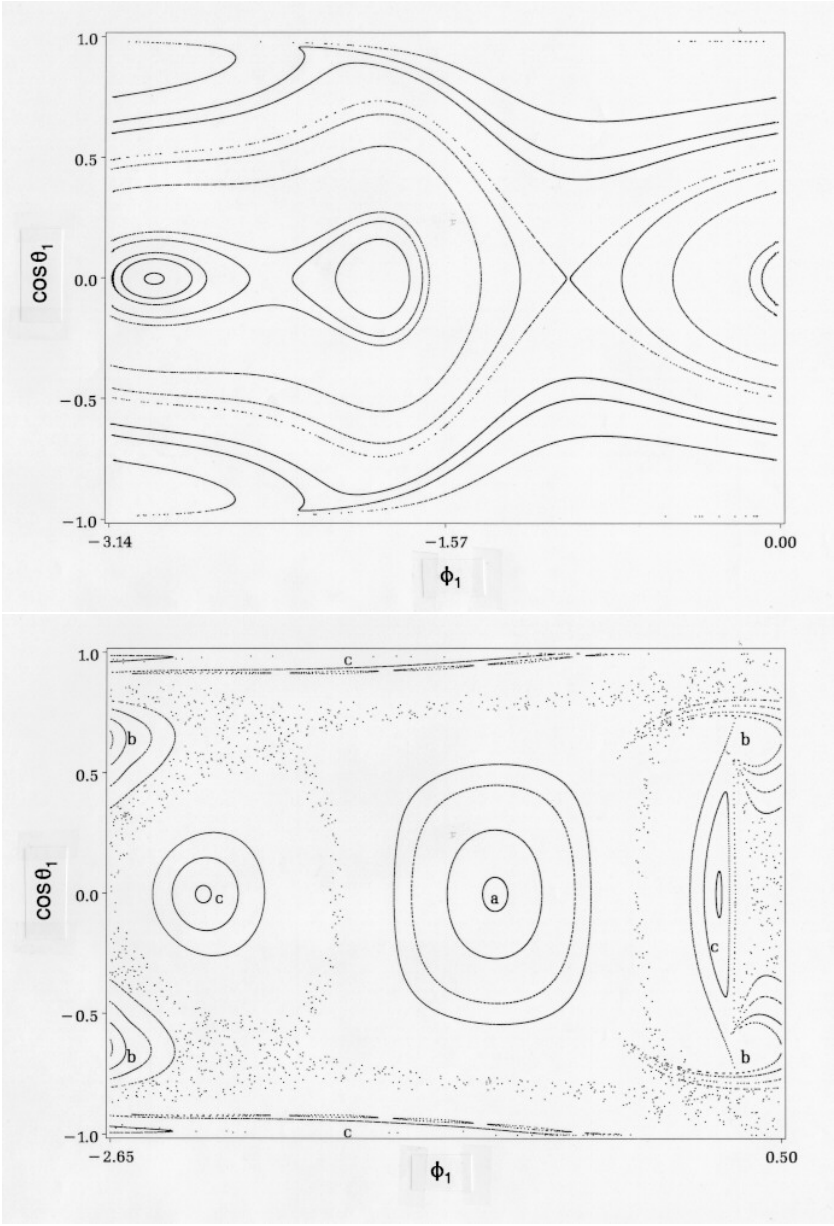

Figure 3: Poincaré surface of section ($p_2 = 0, \dot{p}_2 > 0$) projected onto the (p_1, q_1)-plane of several phase-space trajectories at energy $E = 0.2$ for the classical two-spin model (8). The parameters for the integrable case (a) are $J_x = 1.2, J_y = 0.8, J_z = 0, A_x = A_y = A_z = 0$; the parameters for the nonintegrable case (b) are $J_x = J_y = 1, J_z = 0, A_x = -A_y = -0.7, A_z = 0$.

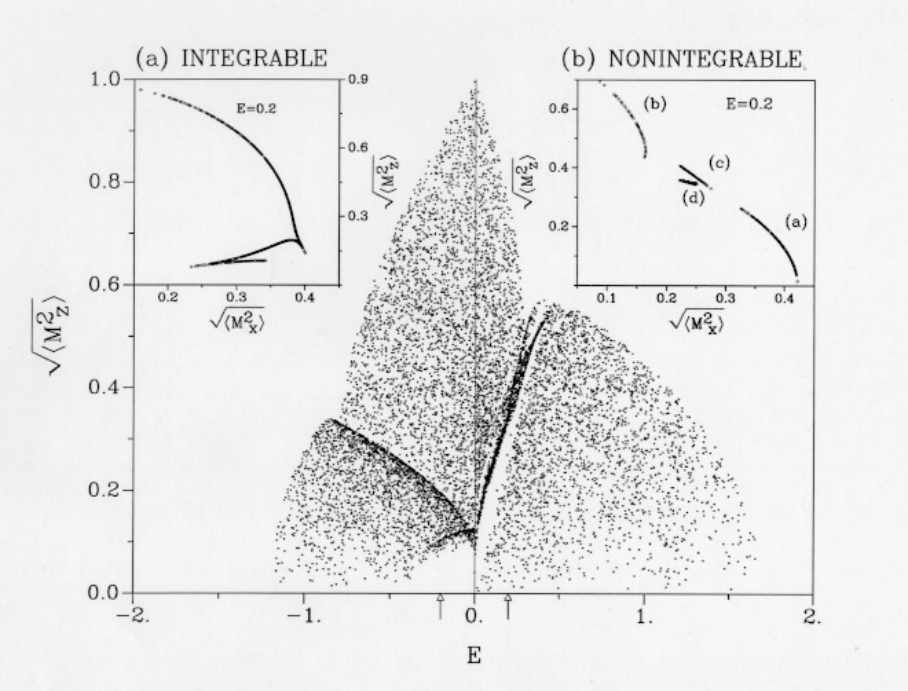

Figure 4: (a) The invariant-surface $E(\tilde{M}_x, \tilde{M}_z)$ projected onto the $(E, \tilde{M}_z)$-plane for the integrable case (see Fig. 3) of the classical two-spin model (8). The inset shows $\tilde{M}_z$ versus $\tilde{M}_x$ at energy $E = 0.2$. The data points represent time averages (9) over individual trajectories for initial conditions randomly chosen in phase space (main plot) or on the energy hypersurface (inset). The number of data points is 5146 (projection, main plot) and 1200 (section, inset). (b) Remnant of the invariant-surface $E(\tilde{M}_x, \tilde{M}_z)$ projected onto the $(E, \tilde{M}_z)$-plane for the nonintegrable case (see Fig. 3). The inset shows $\tilde{M}_z$ versus $\tilde{M}_x$ at energy $E = 0.2$. The data points represent time averages (10) over individual trajectories for initial conditions randomly chosen in phase space (main plot) or on the energy hypersurface (inset). The number of data points is 5050 (projection, main plot) and 495 (section, inset). In both cases the results of a small number of time averages were discarded because of very poor convergence.

Let us summarize the main results for integrable classical systems with two degrees of freedom:

- Every invariant torus is specified by exactly two analytic invariants. These invariants can include the actions J_1, J_2, the energy E, or any invariant obtained from time averages (9) of dynamical variables.
- The relationship between any three such invariants is expressible in terms of a piecewise smooth function of two variables, such as $E(\tilde{M}_x, \tilde{M}_z)$ or $I_A(J_1, J_2)$.

What happens to the Poincaré map and the invariant-surface if integrability is destroyed? This case is illustrated in Figs. 3b and 4b for the nonintegrable case $J_x = J_y = 1, J_z = 0, -A_x = A_y = 0.7, A_z = 0$. The Poincaré map, shown in Fig. 3b, consists predominantly of chaos and different kinds of surviving tori. Not surprisingly, the meltdown of tori into streams of chaos has a dramatic impact on the equation of state between analytic invariants.

When we determine the time averages $\tilde{M}_x$ and $\tilde{M}_z$ for a large number of (regular or chaotic) trajectories with randomly chosen initial conditions, we find that the points $(\tilde{M}_x, \tilde{M}_z, E)$ no longer fall onto a piecewise smooth surface. That surface has partially disintegrated. Fig. 4b shows 5050 such data points projected onto the $(E, \tilde{M}_z)$-plane. For a better perspective, the inset to Fig. 4b shows the section at $E = 0.2$ (indicated by an arrow) of the unprojected remnant of the invariant-surface. The labels (a), (b), (c) relate three different types of invariant tori in Fig. 3b to three distinct pieces of the invariant-surface shown in the inset to Fig. 4b. The cluster of points labeled (d) in Fig. 4b originates from initial conditions in the region of widespread chaos in Fig. 3b.

The invariant-surface is no longer perfectly smooth in any region no matter how small. On the section at $E = 0.2$, we can observe one large interruption separating the fragments marked (a) and (b). This interruption is due to a band of chaos along a separatrix. On both sides of the band, the phase flow is fairly regular, reflected in the seemingly smooth pieces of invariant-surface labeled (a) and (b). In the gap between the two regular regions, a third piece of surface, labeled (c), can be identified. It has its origin in secondary tori (island chains populating the chaotic band).

For initial conditions within this chaotic region, the points $(\tilde{M}_x, \tilde{M}_z)$ tend to cluster at (d) near the center of the gap between the two major remnants of the invariant-surface. Ideally, the entire chaotic region should be represented by a single isolated point in the constant-energy section of the invariant-surface, but time averages along chaotic trajectories tend to converge very slowly.[2] Hence the data points spread into a cluster.

The characteristic pattern is that fragments of the invariant-surface are interrupted by gaps and the gaps are populated by isolated clusters and new pieces of invariant-surface. On the largest scale, this pattern is directly observable in Fig. 4b, but the same pattern repeats itself on smaller scales *ad infinitum*. Not a single piece of smooth surface stays intact. This behavior is characteristic of nonintegrable classical systems with two degrees of freedom. In part III, we shall show how these striking classical nonintegrability effects translate into quantum mechanics. Stay tuned!

Suggestions for further study

1. For small-amplitude oscillations, the simple pendulum behaves like a simple harmonic oscillator, $H = p^2/2m + kx^2/2$. Find the functions $I_K(E) = <\frac{1}{2}m\dot{x}^2(t)>$ and $J(E)$ analytically using (5) and (6), respectively. Plot the results as in Fig. 2 and compare them with the corresponding results for the simple pendulum. Quantize the action for the harmonic oscillator according to the prescription $J_n = n\hbar + \alpha,\ n = 0, 1, 2, \ldots$ with $\alpha = \hbar/2$.

Use the quantized values of J with your graph to determine the corresponding values of the energy and the average kinetic energy. Use the same quantized actions, i.e., the same value for α, for the simple pendulum and determine its quantum spectrum for librational motion. Compare these predictions of semiclassical quantization with those obtained directly from the eigenvalues of the time-independent Schrödinger equation, and the expectation values of the kinetic-energy operator, respectively.

2. Replace the potential $\Gamma(1 - \cos q)$ in (3) by a square well, $V(q) = 0$ if $|q| < q_0$ and $V(q) = V_0$ if $q_0 < |q| < \pi$. Produce the equivalent of Fig. 2 by analytic and/or numerical integrations using (5) and (6). Compare your results with those for the simple pendulum. What happens to the period of oscillation near the separatrix? Compare the semiclassical energy-level spacings with the well-known results for the quantum square well.

3. Consider a particle in a $2d$ square box of linear dimension L. Compute the long-time averages $<{p_x}^2>$ and $<{p_y}^2>$ as in (9) for many randomly chosen initial conditions. Plot $\tilde{p}_x \equiv <{p_x}^2>$ versus $\tilde{p}_y \equiv <{p_y}^2>$ for a fixed value of the energy E as in the inset of Fig. 4a. Explain the shape of the line on which all data points fall. Find an analytic expression for the equation of state (10), i.e., $E = E(\tilde{p}_x, \tilde{p}_y)$.

4. Consider a particle of unit mass moving in the xy-plane subject to the Hénon-Heiles potential $V(x, y) = x^2 y - \frac{1}{3}y^3 + \frac{1}{2}(x^2 + y^2)$. This system exhibits both regular and chaotic orbits. For energy $E = 0.05$, regular orbits are predominant; $E = 0.125$ gives a mixture of regular and chaotic orbits; as E is increased, a larger and larger fraction of initial conditions leads to chaotic orbits. Choose a value of E and compute the long-time averages $\tilde{p}_x$ and $\tilde{p}_y$ as in (9) for many randomly chosen initial conditions. Plot $\tilde{p}_x$ versus $\tilde{p}_y$ and compare your results with the observations made in the context of Fig. 4b.

5. Consider the potential $V(x, y) = \frac{1}{2}x^2 y^2$ and repeat all the computations for energy $E = 0.5$. Almost all data points in a $(\tilde{p}_x, \tilde{p}_y)$ plot produce a single cluster. See ref. 6 for an explanation.

Quantum chaos research at URI is supported by the National Science Foundation, Grant DMR-90-07540. Access to supercomputers at the National Center for Supercomputing Applications, University of Illinois at Urbana-Champaign and at the NASA Ames Research Center is gratefully acknowledged. We thank Harvey Gould and Jan Tobochnik for helpful suggestions.

References

1. N. Srivastava, C. Kaufman and G. Müller, *Computers in Physics* **4**, 549 (1990).

2. N. Srivastava, C. Kaufman, G. Müller, R. Weber, and H. Thomas, *Z. Phys.* B **70**, 251 (1988).

3. N. Srivastava and G. Müller, *Z. Phys.* B **81**, 137 (1990).

4. H. Goldstein, *Classical Mechanics*, Addison-Wesley, (1980) (graduate text); I. Percival and D. Richards, *Introduction to Dynamics*, Cambridge University Press (1982) (undergraduate text); M. Tabor, *Chaos and Integrability in Nonlinear Dynamics*, Wiley (1989) (monograph).

5. E. Magyari, H. Thomas, R. Weber, C. Kaufman and G. Müller, *Z. Phys.* B **65**, 363 (1987).

6. P. Dahlqvist and G. Russberg, *Phys. Rev. Lett.* **65**, 2837 (1990).